Published in final edited form as:
J Biomech. 2015 February 26; 48(4): 708–711. doi:10.1016/j.jbiomech.2015.01.014.

Microstructural and mechanical characterization of scarred vocal folds

Hossein K. Heris[a], **Amir K. Miri**[a,*], **Nageswara R. Ghattamaneni**[b], **Nicole Y.K. Li**[c], **Susan L. Thibeault**[c], **Paul W. Wiseman**[b], and **Luc Mongeau**[a]

[a]Biomechanics Laboratory, Department of Mechanical Engineering, McGill University, 817 rue Sherbrooke Ouest, Montreal, QC, Canada H3A 0C3

[b]Physics and Chemistry Departments, McGill University, 3600 rue University, Montreal, QC, Canada H3A 2T8

[c]Division of Otolaryngology—Head and Neck Surgery, Department of Surgery, University of Wisconsin, Madison, WI 53792, United States

Abstract

The goal of this study was to characterize the vocal folds microstructure and elasticity using nonlinear laser scanning microscopy and atomic force microscopy-based indentation, respectively. As a pilot study, the vocal folds of fourteen rats were unilaterally injured by full removal of lamina propria; the uninjured folds of the same animals served as controls. The area fraction of collagen fibrils was found to be greater in scarred tissues two months after injury than the uninjured controls. A novel mathematical model was also proposed to relate collagen concentration and tissue bulk modulus. This work presents a first step towards systematic investigation of microstructural and mechanical characteristics in scarred vocal fold tissue.

Keywords

Vocal fold; Atomic force microscopy; Scarring; Second harmonic generation

1. Introduction

Vocal fold scars can result from the surgical removal of benign or malignant vocal fold lesions, phonotrauma or intubation over an extended period of time (Benninger et al., 1996; Rosen, 2000). Changes in the microstructure and elasticity of the vocal fold lamina propria (LP) hampers the oscillations of the vocal folds. Mechanical injury triggers a cascade of inflammation and healing response, followed by tissue restoration. During wound

*Correspondence to: Mining and Materials Engineering Department, McGill University, 817 Sherbrooke Street West, Montreal, QC, Canada H3A 2B2. Tel.: +1 514 661 1363. amir.miriramsheh@mail.mcgill.ca (A.K. Miri).

Conflict of interest statement
None.

Uncited references
Bischoff et al. (2000), Hiermaier (2008), Lin et al. (2007), Miri et al. (2012a).

remodeling, the last phase of the healing process, the extracellular matrix (ECM) of the granulation tissue is reorganized dynamically over months to develop into a mature scar (Hansen and Thibeault, 2006). The concentration, organization, and morphology of collagen, one of the main constituents of the ECM, determine wound stiffness. Published animal studies have shown that collagen is first observed in day 1 (collagen type III) and day 2 (collagen type I) following the surgical removal of the rat LP (Tateya et al., 2006). Total collagen levels peak at weeks 2 and 4, respectively, and then decline to become stable in the period between weeks 8 and 12 (Tateya et al., 2005). Evidence suggests that the remodeling phase in rat vocal fold wounds starts at day 7, undergoes an active remodeling phase between weeks 2 and 4, and reaches a stable remodeling phase at week 8 (Tateya et al., 2005, 2006).

Changes in collagen morphology alter the tissue elasticity, as manifested by a change in displacement response under tensile loading (Miri et al., 2013). Data reported from animal studies to date include the concentration of structural constituents from immunohistochemistry (IHC) or molecular data (e.g., see Tateya et al., 2006). The IHC methods require time-consuming sample preparation and tissue slicing, which may alter the organization of the collagen fibrils. In the present study, nonlinear laser scanning microscopy (NLSM) based on second harmonic generation (SHG) imaging (Miri et al., 2012b) was used to investigate the morphological changes of collagen in scarred rat vocal folds without physical sectioning of the tissue. Atomic force microscopy (AFM) was also used to quantify the elastic properties of vocal folds through indentation tests. AFM has been utilized for structural characterization at nano and microscales to examine the morphology and elasticity of LP collagen fibrils, as well as the overall elasticity, adhesion, and surface roughness of the LP (Heris et al., 2013; Johanes et al., 2011; Miri et al., 2013). Miri et al. (2013) showed the applicability of AFM and NLSM for better understanding structure-function relationships (and hyperelastic modeling) of normal vocal folds. The present work aimed to use the combination of AFM and NLSM, along with mathematical modeling based on the eight-chain polymer model, to characterize vocal fold scarring. This may provide new insights into the role of collagen remodeling in wound healing.

2. Methods and materials

2.1. Surgical procedures and sample preparation

The animal study was approved by the Institutional Animal Care and Use Committee of the University of Wisconsin-Madison (protocol number MO2358). Vocal fold injuries were created in fourteen Sprague-Dawley adult male rats (4 to 6 months old; 450 to 500 g) following an established protocol (Welham et al., 2009). Briefly, animals were anesthetized and their vocal folds were injured unilaterally using a 25G needle to remove the vocal fold LP. The uninjured side of the vocal fold served as control. Animals were euthanized for laryngeal harvest at one and two months after surgery. For each time point, one of the seven larynges was fixed in 10% neutral formalin for histological analysis. Hematoxylin and eosin (H&E) staining was performed to evaluate the changes in overall vocal fold morphology over time. The remaining six larynges were dissected to extract vocal fold mucosa for AFM indentation analysis. Animals were euthanized via CO2 asphyxiation. Total laryngectomy

was performed immediately following euthanasia. For each larynx, the vocal fold mucosa was dissected from the thyroarytenoid muscle under a stereo dissection microscope. A portion of the arytenoid cartilages was included in the samples to help establish indentation orientation.

A small layer of nail polish was applied on a glass coverslip. Each sample was placed on one coverslip with the marked side of the tissue facing towards the substrate. The other side of the tissue was used for indentation tests. For NLSM imaging, the samples were fixed in formalin for 6 h and were then placed in a phosphate buffer solution (pH=7.6) overnight.

2.2. Atomic force microscopy based indention

Indentation tests were performed using a Veeco multimode atomic force microscope with a NanoScope V controller. Colloidal probes were purchased from Novascan technologies Inc. (Ames, IA, USA) with a nominal stiffness of 7.5 N/m and a probe diameter of 25 μm. A thermal tuning method was used to calibrate stiffness of the cantilevers (Heris et al., 2013). Three areas of 100 μm ×100 μm were indented around the center of each sample. A liquid cell for the AFM cantilever was used to perform the experiments in buffer solution at room temperature. Samples (n=2±1 per group) with muscle infiltration, visible in NLSM images, were not used for indentation tests. Samples (n=4±1 per group) were indented using a ramp function, with 4 μm/s loading and unloading rate. Unloading was initiated immediately after the maximum load was reached. To minimize the influence of possible permanent deformations, the unloading data were used as a basis for the determination of the indentation elastic modulus. A model previously reported in Heris et al. (2013) was used to infer elastic properties from the measured data.

2.3. Nonlinear laser scanning microscopy

A custom built multi-modal nonlinear laser scanning microscope was used to perform optical sectioning imaging of the control and scar samples. Details of the setup can be found in a published protocol (Miri et al., 2012b). Excitation ultrafast pulsed laser beams were generated using an objective focused with a wavelength of ~1050 nm (linear polarization) and a pulse duration of ~100 fs, inducing a laser power of 30–150 mW (before the collection objective) depending on the sample thickness and density. The laser power was adjusted in such a way that the brightest pixels were just below the level of saturation. Because the large power intensity indicates significant scattering and absorption of light within the samples, varying the laser power dictated some extent of uncertainties that can violate the consistency of SHG imaging (the SHG power has a quadratic dependence on the laser power). The excitation and collection objectives (Carl Zeiss, Toronto, Canada) were a 63 ×0.9 NA water immersion lens with a 2 mm working distance and a 20 ×0.80 NA water immersion lens with a 0.61 mm working distance, respectively. The SHG images were accumulated sequentially with single point PMT detection in the forward direction. The pixel dwell time was about 5 ms, yielding a total scanning time of ~250 s (for a case of 5-frame averaging). Over five random areas of 130 μm ×130 μm were scanned in each biopsy (at depths from 0.5 to 1.5 mm) and used for image analysis. The depth variation associated with arbitrarily shaped biopsies may increase the level of uncertainty in the quantitative analysis. Two parameters, H_0 and R_0, corresponding to the periodicity and amplitude of the presumably

sinusoidal fibers/fibrils were estimated from the NSLM images via the image analysis used by Miri et al. (2012b). Fourier analysis was used to determine the periodicity of selected collagen bundles. ImageJ (NIH, Bethesda, MD, USA) was used to calculate the area fraction of collagen fibrils in each image by imposing a binary threshold, following background subtraction. Another ImageJ plug-in, designed based on the algorithm in Liu (1991), was used to measure the dispersion (i.e., the directionality of fiber distribution) of fibrils' orientations within 100 μm × 100 μm regions.

All data reported in this paper are presented as mean values with their standard deviations. Data were analyzed with Excel (Microsoft, Redmond, WA). For comparison of groups, we used two-way ANOVA with repeated measures with the two factors being time and treatment. Differences with *p*-values of less than 0.05 were considered statistically significant.

3. Results

LP removal and associated scarring was first confirmed using standard H&E, as shown in Fig. 1. One month after surgery (Fig. 1a), the scarred vocal fold appeared to have an irregular shape, with a complete epithelium and a fibrous LP. Two months after surgery (Fig. 1b), the gross morphology of the scarred vocal fold approximated that of its uninjured control. Table 1 shows the elastic modulus of uninjured normal controls and injured vocal folds. The statistical differences between elastic moduli of uninjured control samples (250±140 kPa and 240±130 kPa) and those of scarred samples (160±60 kPa and 380±160 kPa) were insignificant (p=0.61; two-way ANOVA). However, the average elastic moduli at one-month scarring (160±60 kPa) was smaller than those at two-month scarring (380±160 kPa) when compared using two-tailed Student's *t*-test (p=0.09).

The SHG images of both scarred and uninjured tissue are shown in Fig. 2, illustrating the evolution of scared tissue. The area fraction of collagen fibrils and their morphological properties, such as their periodicity, amplitude, and dispersion are shown in Table 2. In general, all data were consistent between one-month and two-month uninjured controls. The two-way ANOVA revealed an overall significant increase in collagen area fractions by scarring (p=0.006). The collagen area fractions in one-month and two-month scarring were respectively 35.4±2.4% and 36.9±4.5%, greater than control samples (28.7±6.6% and 29.6±2.6%). There was no marked difference observed in timing between one-month and two-month groups (p=0.58; two-way ANOVA), as expected from rapid wound healing in rats. Although the average values of amplitude and periodicity were greater for uninjured tissue than one-month scarring, there was no significant difference (p=0.64 and p=0.75). There was also a significant decrease in dispersion values by scarring (23.3±5.8° and 21.6±3.5° in the scarred group vs. 32.1±2.0° and 29.1±4.7° in the control group; p=0.003 from two-way ANOVA).

4. Concluding remarks

The indentation elastic modulus of the uninjured rat LP (250±140 kPa) is much greater than the indentation elastic modulus of porcine LP (3–5 kPa; Heris et al., 2013) and that of the human LP (4–6 kPa; Chhetri et al., 2011). The higher modulus explains why vocalization in

rats falls within the ultrasonic-range. The phonatory fundamental frequency of rats (2–4 kHz; Nitschke, 1982) is one order of magnitude greater than that of humans (100–300 Hz; Titze et al., 2003). Contrary to expectations, the differences of indentation moduli between uninjured and scarred rat vocal fold samples were found to be statistically insignificant. In addition to the low number of samples available, this fact could be due to the intrinsic uncertainties associated with the use of AFM and the testing protocol. First, surface roughness of the vocal fold biopsies can cause significant errors on AFM-based indentation results. Second, muscle infiltration present in some of the biopsies can distort the results although the SHG marker of myosin was used to exclude any cases with muscle infiltration. Third, the anisotropy of vocal fold tissue and the directionality of scar progression (please see Fig. 2) may yield significant deviations in the Hertz contact theory. The physical heterogeneity of the rat vocal folds may also contribute to variability in a local mechanical testing method, such as AFM-based indentation.

The microscale helical shape of the collagen fibrils, also known as “crimp pattern”, plays an important role in the nonlinearity of tissue elasticity (Miri et al., 2013, 2012b). A large waviness implies a high threshold stretch required for the onset of strain stiffening. The collagen area fraction, periodicity, and amplitude are respectively different in rats (~30%, ~10 μm, ~1 μm), pigs (~15%, ~30 μm, ~4 μm; Miri et al., 2013), and humans (~15%, ~30 μm, ~3 μm Miri et al., 2012b). Collagen area fractions in rats are significantly higher than in humans and pigs. Human and porcine vocal folds have a similar collagen area fraction (~15%) as well as elastic properties (Chhetri et al., 2011; Heris et al., 2013). In soft tissues with unidirectional collagen fibrils such as tendons, a decrease in the crimp angle (i.e., the slope of sinusoidal fibril at the origin) and amplitude was found to make the tissue mechanically weaker, with lower elastic modulus (Wang, 2006; Wilmink et al., 1992). Lower crimp angles in one-month scarring (~31±4°) compared to two-month scarring (~35±5°) can possibly be related to immature collagen fibrils generated during the early phase of fibrosis. The dispersion of collagen fibrils in scarred vocal fold tissue was lower than in uninjured controls as shown in Table 2. The lower dispersion might be related to a contraction of the wound along the anterior–posterior direction during early healing, as well as tissue stretching along the anterior–posterior direction during rat vocalization. The dispersion of the collagen fibrils decreased from one month to two months. Such changes might be related to the neo-synthesis of collagen which had undergone remodeling in the wound area.

A mathematical model is presented in Appendix A to relate the indentation elastic modulus, collagen fibrillar density, and the degree of collagen crosslinking. Based on the model, the elastic moduli of tissues with an equal concentration of collagen can vary more due to the degree of crosslinking and structural configurations than simply the concentration of collagen fibrils. However, the low statistical significance of the mechanical data prevents any conclusions regarding the structure-function relations. The experimental and theoretical methods presented in this work can be applied to assess the performance of tissue-engineered constructs for future applications. The local characterization of a biological tissue is critical in applications where an injectable biomaterial is applied locally to repair or regenerate a damaged portion. The structural evolution of the engineered tissue construct

can be also imaged using NLSM and related to bulk elasticity of the construct through the model.

Supplementary Material

Refer to Web version on PubMed Central for supplementary material.

Acknowledgments

The work has been supported by the National Institute on Deafness and Other Communication Disorders, grant DC 005788 (L. Mongeau, PI), DC 004336 (S. Thibeault, PI), DC012112 (N. Li, PI). PWW acknowledges support from a Natural Sciences and Engineering Council of Canada (NSERC) Discovery Grant support and the Canada Foundation for Innovation (CFI). The authors would like to express their gratitude to Prof. François Barthelat (Mechanical Engineering Department, McGill University, Montreal) for sharing his atomic force microscope.

References

Benninger MS, Alessi D, Archer S, Bastian R, Ford C, Koufman J, Sataloff RT, Spiegel JR, Woo P. Vocal fold scarring: current concepts and management. Otolaryngol Head Neck Surg. 1996; 115:474–482. [PubMed: 8903451]

Bischoff JE, Arruda EM, Grosh K. Finite element modeling of human skin using an isotropic, nonlinear elastic constitutive model. J Biomech. 2000; 33:645–652. [PubMed: 10807984]

Chhetri DK, Zhang Z, Neubauer J. Measurement of Young's modulus of vocal folds by indentation. J Voice. 2011; 25:1–7. [PubMed: 20171829]

Hansen JK, Thibeault SL. Current understanding and review of the literature: vocal fold scarring. J Voice. 2006; 20:110–120. [PubMed: 15964741]

Heris HK, Miri AK, Tripathy U, Barthelat F, Mongeau L. Indentation of poroviscoelastic vocal fold tissue using an atomic force microscope. J Mech Behav Biomed Mater. 2013; 28:383–392. [PubMed: 23829979]

Hiermaier, S. Structures Under Crash and Impact: Continuum Mechanics, Discretization and Experimental Characterization. Springer; 2008.

Johanes I, Mihelc E, Sivasankar M, Ivanisevic A. Morphological properties of collagen fibers in porcine lamina propria. J Voice. 2011; 25:254–257. [PubMed: 20171830]

Lin D, Dimitriadis E, Horkay F. Elasticity of rubber-like materials measured by AFM nanoindentation. Express Polym Lett. 2007; 1:576–584.

Liu ZQ. Scale space approach to directional analysis of images. Appl Opt. 1991; 30:1369–1373. [PubMed: 20700292]

Miri AK, Barthelat F, Mongeau L. Effects of dehydration on the viscoelastic properties of vocal folds in large deformations. J Voice. 2012a; 26:688–697. [PubMed: 22483778]

Miri AK, Heris HK, Tripathy U, Wiseman PW, Mongeau L. Microstructural characterization of vocal folds toward a strain-energy model of collagen remodeling. Acta Biomater. 2013; 9:7957–7967. [PubMed: 23643604]

Miri AK, Tripathy U, Mongeau L, Wiseman PW. Nonlinear laser scanning microscopy of human vocal folds. Laryngoscope. 2012b; 122:356–363. [PubMed: 22252839]

Nitschke, W. Acoustic behavior in the rat: research, theory, and applications. Praeger; 1982.

Rosen, CA. Vocal fold scar. In: Rosen, CA.; Murry, T., editors. The Otolaryngologica Clinics of North America. Voice Disorders and Phonosurgery. W.B. Saunders; Philadelphia: 2000.

Tateya T, Tateya I, Sohn JH, Bless DM. Histologic characterization of rat vocal fold scarring. Ann Otol Rhinol Laryngol. 2005; 114:183–191. [PubMed: 15825566]

Tateya T, Tateya I, Sohn JH, Bless DM. Histological study of acute vocal fold injury in a rat model. Ann Otol Rhinol Laryngol. 2006; 115:285–292. [PubMed: 16676825]

Titze IR, Švec JG, Popolo PS. Vocal dose measures: quantifying accumulated vibration exposure in vocal fold tissues. J Speech Lang Hear Res. 2003; 46:919–932. [PubMed: 12959470]

Wang JHC. Mechanobiology of tendon. J Biomech. 2006; 39:1563–1582. [PubMed: 16000201]

Welham NV, Montequin DW, Tateya I, Tateya T, Choi SH, Bless DM. A rat excised larynx model of vocal fold scar. J Speech Lang Hear Res. 2009; 52:1008–1020. [PubMed: 19641079]

Wilmink J, Wilson AM, Goodship AE. Functional significance of the morphology and micromechanics of collagen fibres in relation to partial rupture of the superficial digital flexor tendon in racehorses. Res Vet Sci. 1992; 53:354–359. [PubMed: 1465509]

Appendix A. Supporting information

Supplementary data associated with this article can be found in the online version at http://dx.doi.org/10.1016/j.jbiomech.2015.01.014.

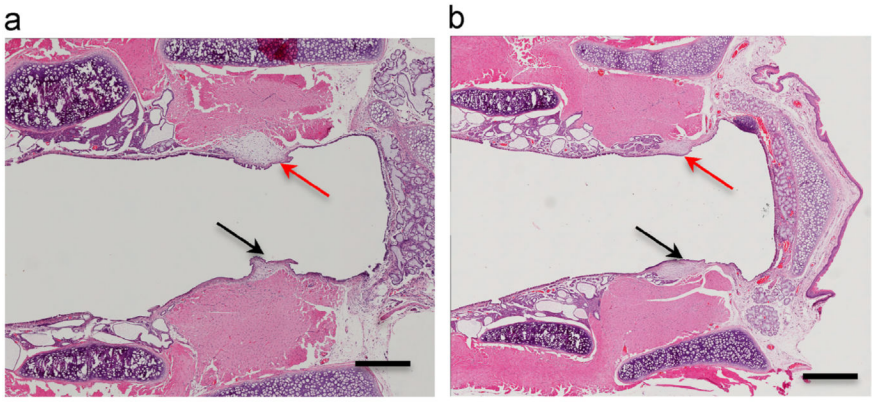

Fig. 1.

Histological staining of rat vocal fold tissue. Red arrows indicate normal vocal folds. Injured vocal folds are indicated by black arrow. (a) One-month post injury. (b) Two-month post injury. Scale bar is 500 μm. (For interpretation of the references to color in this figure legend, the reader is referred to the web version of this article.)

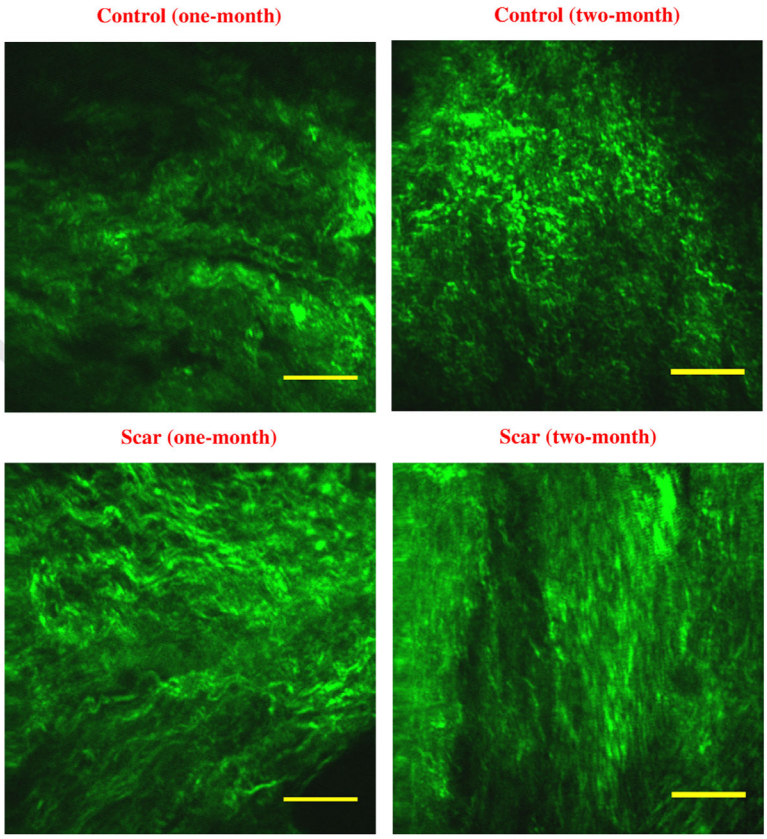

Fig. 2.

Representative second harmonic generation microscopy images of collagen distribution in normal (top row) and scarred vocal folds (bottom row) in one-month (1st column) and two-month (2nd column) after scarring. Scale bar is 20 μm.

Table 1

Mean indentation elastic modulus (kPa) of control and injured rat vocal fold lamina propria tissue for one month and two months post injury.

One-month control	One-month scarring	Two-month control	Two-month scarring
245±144	164±61	241±125	375±163

Table 2

Area fraction and morphological characteristics of collagen fibrils.

Parameter	One-month control	One-month scarring	Two-month control	Two-month scarring
Amplitude (μm)	1.1±0.6	0.8±0.3	1.1±0.5	1.2±0.3
Periodicity (μm)	9.9±5.4	8.6±1.4	10.2±4.4	11.2±4.0
Area fraction (%)	28.7±6.6	35.4±2.4	29.6±2.6	36.9±4.5
Dispersion (°)	32.1±2.0	23.3±5.8	29.1±4.7	21.6±3.5